Chemical Engineering Journal 284 (2016) 93–102

Contents lists available at ScienceDirect

Chemical Engineering Journal

journal homepage: www.elsevier.com/locate/cej

Removal of 17β-estradiol by few-layered graphene oxide nanosheets from aqueous solutions: External influence and adsorption mechanism

Lu-hua Jiang [a,b], Yun-guo Liu [a,b,*], Guang-ming Zeng [a,b], Fang-yu Xiao [a,b], Xin-jiang Hu [a,b], Xi Hu [c], Hui Wang [a,b], Ting-ting Li [a,b], Lu Zhou [a,b], Xiao-fei Tan [a,b]

[a] College of Environmental Science and Engineering, Hunan University, Changsha 410082, PR China
[b] Key Laboratory of Environmental Biology and Pollution Control (Hunan University), Ministry of Education, Changsha 410082, PR China
[c] College of Environmental Science and Engineering Research, Central South University of Forestry and Technology, Changsha 410004, PR China

HIGHLIGHTS

- The maximum adsorption capacity of E2 onto GO was 149.4 mg/g at 298 K and pH 7.0.
- The adsorption process was characterized by kinetics, isotherm and thermodynamic analysis.
- The E2 adsorption onto GO worked well in the presence of NaCl.
- GO still remained excellent adsorption capacity after numerous desorption/adsorption cycles.
- The adsorption mechanism was believed to be π–π interactions and hydrogen bonds between GO and E2.

GRAPHICAL ABSTRACT

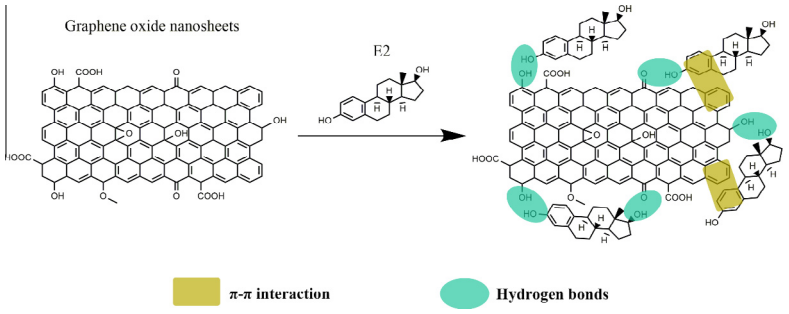

ARTICLE INFO

Article history:
Received 23 June 2015
Received in revised form 26 August 2015
Accepted 28 August 2015
Available online 3 September 2015

Keywords:
Endocrine disrupting chemicals
17β-estradiol
Graphene oxide nanosheets
Adsorption
π–π interaction

ABSTRACT

This study demonstrates the use of few-layered graphene oxide nanosheets (GO) as efficient adsorbents for the removal of 17β-Estradiol (E2) from aqueous solutions via strong adsorptive interactions. The adsorption performance of GO was investigated by batch adsorption experiments. Further, adsorption experiments were carried out in the presence of other environmental pollutants to understand external influence on the adsorption of E2 by GO. The result indicated that the maximum adsorption capacity (q_m) of GO for E2 obtained from the Langmuir isotherm was 149.4 mg/g at 298 K and it was the highest values of E2 adsorption compared to that of other adsorbents reported before. Thermodynamic study indicated that the adsorption was a spontaneous process. In addition, the result showed that E2 adsorption on GO was slight affected by the solution pH. The presence of NaCl in the solution facilitated the E2 adsorption and the optimum adsorption capacity was obtained when the NaCl concentration was 0.001 M. Moreover, the effect of background electrolyte divalent cations (Mg^{2+} and Ca^{2+}) was not similar with the monovalent cations (Na^{+} and K^{+}). While the influence of background electrolyte anions (Cl^{-}, NO_3^{-}, SO_4^{2-}, and PO_4^{3-}) were not significantly different. The presence of humic acid reduced E2 adsorption on GO at pH 7.0. GO still exhibited excellent adsorption capacity following numerous desorption/adsorption cycles. Besides, both π–π interactions and hydrogen bonds might be responsible for the adsorption of E2 onto GO.

1. Introduction

Endocrine disrupting chemicals (EDCs) were prevalent detected in the aquatic environment [1] as well as in drinking water [2], which make EDCs drawn great concern in recent years.

* Corresponding author at: College of Environmental Science and Engineering, Hunan University, Changsha 410082, PR China. Tel.: +86 731 88649208; fax: +86 731 88822829.
E-mail address: liuyunguo_hnu@163.com (Y.-g. Liu).

http://dx.doi.org/10.1016/j.cej.2015.08.139
1385-8947/

17β-Estradiol (E2), the major and most potent form of natural estrogens, has been identified as the unique environmental concern among EDCs because they are capable of triggering negative responses in aquatic organisms at low concentrations [3]. The adverse effect of E2 on aquatic organisms, including fish egg production inhibition and sex reversal of males, ultimately could result in the collapse of local fish populations [4]. Therefore, it is urgent to put forward some rational and feasible suggestions for E2 pollution control.

In recently, a variety of methods have been explored to decontaminate E2 such as adsorption [5], catalytic degradation [3], photo-catalytic degradation [6], biodegradation [7], and advanced oxidation [8]. Among these various methods, adsorption is a superior and widely used method because of its accessibility, high efficiency and environmentally benign. In fact, a number of sorbent materials have been applied for eliminating E2. Zhang et al. reported that E2 could be adsorptive removed from water via various adsorbents such as granular activated carbon (GAC), chitin, chitosan, ion exchange resin and carbonaceous adsorbent prepared from industrial waste [9]. Yoon et al. investigated adsorption of E2 by several powdered activated carbons (PAC) [10]. Besides, sorbents including single-walled carbon nanotubes [11], multi-walled carbon nanotubes [12], polyamide thin-film composite nanofiltration (NF) membranes [13], and molecularly imprinted polymer [14] were successfully used to adsorption E2 from aqueous systems. However, these sorbents suffer the problem of either low sorption capacities or high-cost. Thus, there is a strongly desire to search for a high-performance, low-cost and reusable adsorbent.

Graphene oxide nanosheets (GO), composed of a single atomic layer of sp^2-hybridized carbon arranged in a honeycomb structure, have unusual properties such as excellent mechanical, optical, and electrochemical properties [15–17]. Therefore, they can be the next-generation nanomaterials to be applied in many fields such as supercapacitors, solar cells and sensors [18–20]. Much of the research in the last few years has proved that GO could be a promising material to adsorb pollutants from water, due to its extremely hydrophilicity, ultrahigh theoretical surface area and abundant surface oxygen-containing groups [21]. In previous study GO was used as an adsorbent for divalent metal ions (copper, zinc, cadmium and lead) removal and the result showed that the adsorption capacity of GO for Cu(II), Zn(II), Cd(II), and Pb(II) could stupendously reach up to 294, 345, 530, and 1119 mg/g, respectively [22]. Pavagadhi et al. demonstrated that GO could act as a good adsorbent in adsorbing microcystin-LR (MC-LR) and microcystin-RR (MC-RR) from aqueous solution [23]. As Yan et al. reported, GO could be employed as an efficient adsorbent for the removal of three aromatic organic compounds (aniline, nitrobenzene, and chlorobenzene) [24]. Moreover, GO have been successful used in adsorption various dyes such as methylene blue [25], Basic Red 12 [26], and triphenylmethane dyes [27] from aqueous. However, its potential application for removal of E2 from aqueous solutions remains unknown.

In the present study, the ability of GO to remove E2 from aqueous solutions was examined for the first time using a series of systematic adsorption and kinetic experiments. The influence of the contact time, E2 concentration, temperature, pH, ionic strength, and humic acid on removal of E2 from aqueous solutions by GO were studied systematically. In addition, the effect of common electrolyte anions (Cl^-, NO_3^-, SO_4^{2-}, and PO_4^{3-}) and electrolyte cations (Na^+, K^+, Mg^{2+} and Ca^{2+}) in aqueous solutions on the adsorption of E2 onto GO was investigated. Five cycles of desorption/regeneration were explored to assess the reusability and cost effectiveness of GO. In addition, the mechanism of GO toward E2 was estimated.

2. Experimental section

2.1. Preparation of few-layered graphene oxide nanosheets

Graphite powder (particle size $\leqslant$ 30 μm) was supplied by Tianjin Kermel Chemical Regent Ltd, China. The water used in experiment is high-purity water (18.25 MΩ/cm) generated by Millipore Milli-Q water purification system. All chemicals including $K_2S_2O_8$, P_2O_5, H_2SO_4, $NaNO_3$, $KMnO_4$, H_2O_2, and HCl were analytical reagent grade and were purchased from Shanghai Chemical Corp.

Few-layered graphene oxide nanosheets were synthesized from natural graphite powder by modified Hummers method [28]. Briefly, graphite powder (6.0 g), $K_2S_2O_8$ (5.0 g) and P_2O_5 (5.0 g) were added into the concentrated H_2SO_4 (24.0 mL) and stirred at 80 °C for 4.5 h. Then, Milli-Q water (1.0 L) was added and left overnight. The mixture was washed thoroughly and dried under vacuum at 60 °C. The residue was collected and dispersed in the cold (0 °C) concentrated H_2SO_4 (240 mL), then $NaNO_3$ (5.0 g) and $KMnO_4$ (30.0 g) were added gradually and the mixture was continually stirred below 20 °C for 4 h. Then, the reaction was carried out at 35 °C for 2 h. Next, Milli-Q water (500 mL) was added slowly and the mixture was stirred for another 6 h at 90 °C. After that, Milli-Q water (1 L) and 30 wt.% H_2O_2 (40 mL) were added to the mixture, and stirred for 2 h at room temperature. After centrifugal, the GO particles were washed repeatedly with HCl (5%) and Milli-Q water to remove the residual metal ions and sulfate ions. Finally, the graphene oxide nanosheets were dried under vacuum at 65 °C.

2.2. Characterization of few-layered graphene oxide nanosheets

The structures and surface morphologies of the samples were characterized by scanning electron microscopy (SEM) (JSM-7001F, Japan) and transmission electron microscopy (TEM) (JEM-3010, Japan) [29]. Atomic force microscopy (AFM) images were carried out using a digital instrumental nanoscope III in tapping mode (Veeco Instruments, USA) [30]. The X-ray diffraction (XRD) on a Bruker AXS D8 Advance diffractometer was used Cu Kα source (λ = 1.541 Å) [31]. Raman spectra were obtained from a LabRAM HR UV Raman spectrometer (JDbin Yvon) [29]. The Brunauer–Emmett–Teller (BET) specific surface area of the samples was characterized by automatic surface analyzer (Quantachrome, USA) [32]. For the zeta potentials analysis, the samples were prepared by ultrasonification of 3 mg GO with 30 mL Milli-Q water and the solution pH was adjusted to different values (3–12) by adding negligible volumes 0.1 M NaOH or HCl. Zeta potential measurements were made with a zeta potential meter (Zetasizer Nano-ZS90, Malvern) [31]. The surface functional groups were observed by X-ray photoelectron spectroscopy (XPS) (Thermo Fisher, USA) and Fourier transform infrared spectrum (FTIR) (Nicolet 5700 Spectrometer) [31].

2.3. Adsorption experiments

E2 ($C_{18}H_{24}O_2$, molecular weight 228.29, 98% in purity) was purchased from Sigma–Aldrich Corp. The stock solution (1000 mg/L) of E2 was prepared by dissolving specific amounts of E2 powder into methanol. The solutions of different E2 concentrations used in batch experiments were obtained through diluting the stock solution. However, the volume of methanol in the spiked stock solution was maintained at less than 0.1% to avoid the cosolvent effect. For all the sorption experiments, 3 mg of GO was added in 30 mL of E2 solution. The pH was adjusted to desired values via adding negligible volumes of NaOH or HCl. All batch sorption experiments were performed in a water bath shaker with a shaking speed of 160 rpm.

After being mixed for 8 h, the mixture was separated by centrifugation at 8000 rpm for 10 min and then the supernatants were filtered through 0.45 μm membrane filters [29,32].

The E2 concentration was measured by An F-4500 fluorescence spectrophotometer (Hitachi, Japan). The excitation source was used 450 W xenon lamp. Both the excitation and emission matrix spectra were collected 5 nm over an excitation range of 200–400 nm and an emission range of 300–500 nm. The fluorescence intensity of E2 was determined at Ex/Em = 280 nm/310 nm. The calibration curve was determined using E2 dissolved in truly dissolved solution at concentrations of 0.05–4.0 mg/L. To eliminate water Raman scatter peaks, the spectra were obtained by subtracting the Milli-Q water blank spectra, recorded under the same conditions [12]. The adsorbed E2 amount was calculated using the difference between the initial and equilibrium concentrations. The adsorption capacity is calculated based on the following equation:

$$q_e = \frac{(C_0 - C_e)V}{m} \quad (1)$$

where C_0 and C_e are the initial and equilibrium concentrations of E2 (mg/L), m is the mass of adsorbent (g) and V is the volume of the solutions (L).

To determine the minimum time required for adsorption equilibrium, the adsorption kinetic studies were conducted. 3 mg of GO was added to 30 mL of 2 mg/L E2 solution at pH 7.0 and 298 K. The remaining concentrations of E2 were analyzed at a predetermined time interval ranging from 0.25 to 12 h.

To get information about the maximum adsorption capacities and the thermodynamic properties, adsorption isotherms of E2 on GO were carried out at pH 7.0 under three different temperature (298, 318, and 338 K). The initial E2 concentrations ranged of 1–16 mg/L.

The effect of initial solution pH on E2 adsorption was studied at initial E2 concentration of 3 mg/L and 298 K. The initial pH range from 3.0 to 12.0 and was adjusted with dilute negligible volumes 0.1 M NaOH or HCl solution.

The effect of ionic strength on the adsorption of E2 was studied by adding NaCl to 3 mg/L E2 solutions containing 3 mg GO with concentrations ranging from 0.005 to 0.1 M at 298 K and pH 7.0.

To investigate the adsorption capacity of GO for E2 in the presence of various background electrolyte ions, 0.01 M NaCl, KCl, $CaCl_2$, $MgCl_2$, $NaNO_3$, Na_2SO_4 and Na_3PO_4 were added into 3 mg/L E2 solutions containing 3 mg GO at 298 K and pH 7.0, respectively.

The effect of humic acid on the adsorption of E2 was studied through adding humic acid to 3 mg/L E2 solutions containing 3 mg GO with concentrations ranging from 0.1 to 1 mg/L at 298 K and pH 7.0.

2.4. Desorption experiments

Desorption/adsorption experiment was conducted as follows: the GO which has been used to remove E2 (3 mg/L) was rinsed with 50 mL 4 wt.% NaOH solution at room temperature. Then, the GO particles transferred into a glass vial containing 50 mL pure acetone and the vial was sealed by aluminum foil, agitated at 298 K and 200 rpm for 24 h [33]. After desorption, the suspension liquid was taken to centrifugation and then diluted in 50 mL deionized water. Above steps were repeated for three times and the final sample was dried at 353 K for reuse. In each cycle of adsorption test, 3 mg recycled GO was added to 30 mL 3 mg/L E2 and was shaken at 298 K for 8 h with pH 7.0.

2.5. Model of data analysis

Two types of kinetic models, the pseudo-first order and pseudo-second order, were used to examined the mechanism of adsorption and potential rate controlling steps [34].

The pseudo-first-order model is given as:

$$\ln(q_e - q_t) = \ln q_e - k_1 t \quad (2)$$

where q_e and q_t are the adsorbed amount of E2 at equilibrium and at different time (mg/g), respectively. k_1 is the rate constant of the pseudo-first-order model of adsorption (1/min).

The pseudo-second-order model can be presented as:

$$\frac{t}{q_t} = \frac{1}{k_2 q_e^2} + \frac{t}{q_e} \quad (3)$$

where q_e and q_t are defined the same as the parameters in the pseudo-first-order model, while k_2 (g/mg min) is the second-order adsorption rate constant.

The Langmuir and Freundlich models were used to fit the adsorption isotherms data [28]. The Langmuir equation is given as:

$$q_e = \frac{K_L q_m C_e}{1 + K_L C_e} \quad (4)$$

where q_e (mg/g) is the equilibrium-sorbed concentration and q_m (mg/g) stand for the maximum adsorption capacity of the adsorbent. C_e (mg/L) is the equilibrium solution phase concentration, while K_L (L/g) is the Langmuir constant.

The following expression describes the Freundlich equation:

$$q_e = K_f C_e^N \quad (5)$$

where q_e and C_e are defined the same as the parameters in the Langmuir equation, K_f [(mg/g)/(mg/L)^N] is the Freundlich affinity coefficient, and N is the exponential coefficient.

Adsorption thermodynamics can reveal the information on the inherent energy change of adsorbent after adsorption and also the mechanism involved in the adsorption process [27]. The thermodynamic parameters including standard free-energy change (ΔG°), standard enthalpy change (ΔH°), and standard entropy change (ΔS°) are calculated at three different temperatures by following equations:

$$\Delta G^\circ = -RT \ln K^\circ \quad (6)$$

$$\ln K^\circ = \frac{\Delta S^\circ}{R} - \frac{\Delta H^\circ}{RT} \quad (7)$$

where R (8.314 J/mol K) is universal gas constant and T (K) is the solution temperature. K° is the adsorption equilibrium constant, calculated by plotting $\ln K_d$ ($K_d = q_e/C_e$) versus C_e and extrapolating C_e to zero.

3. Results and discussion

3.1. Characterization of GO

The graphene oxide nanosheets morphological study was carried out by the SEM and TEM images which are presented in Fig. 1. As can be seen from the SEM image, there are many ripples on the surface of GO due to the scrolling of the nanosheets. The TEM image revealed that GO was basically transparent and many wrinkles primarily located on the edge and formed scrolls. As seen from the AFM image (Fig. 2), the thickness of GO is about 1.21 nm and it is suggested that few-layered graphene oxide nanosheets were formed [35,36]. The nitrogen adsorption–desorption isotherms is shown in Fig. 3(a). The BET analysis indicated that the specific surface areas (SA) and pore diameter of GO were 92 m^2/g

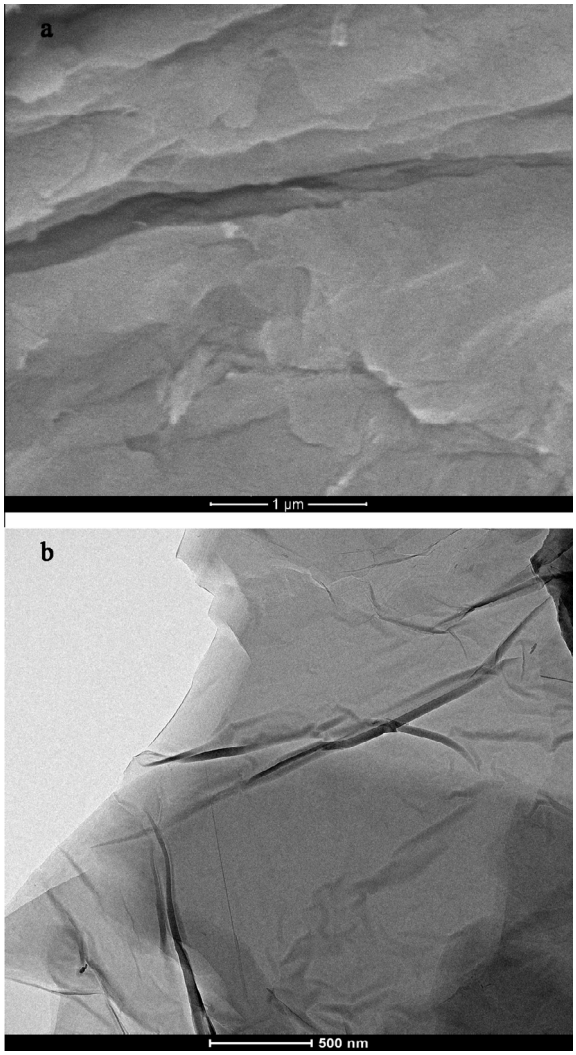

Fig. 1. (a) SEM image of GO; (b) TEM image of GO.

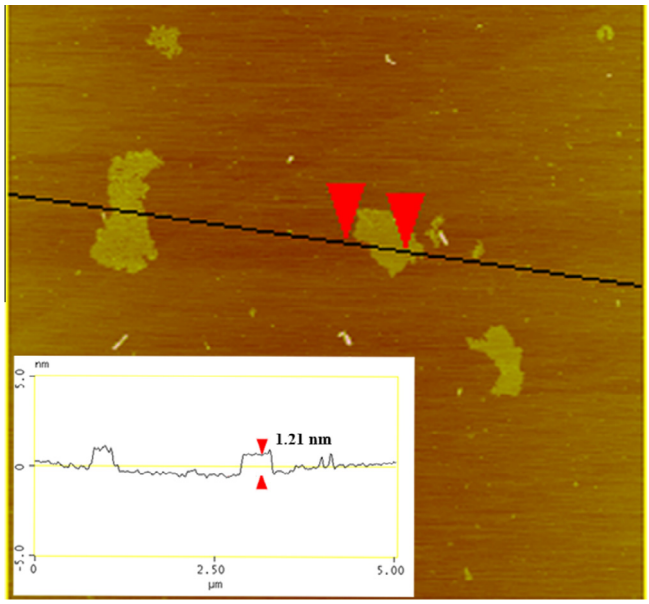

Fig. 2. AFM image of GO.

and 2.69 nm, respectively. The value of the pore diameter suggested that GO was a mesoporous material. Compared with the SA of graphite (4.5 m^2/g) [37], the SA of GO was relatively higher, reflecting an excellent exfoliation degree. However, the obtained value even was much lower than the theoretical value of reduced graphene oxide (rGO) (2620 m^2/g) [29], which may be attributed to the incomplete exfoliation and the agglomerations of graphene oxide layers during the process of sample preparation.

XRD patterns of graphite, GO, and rGO are shown in Fig. 3(b). The XRD pattern of graphite exhibited a sharp and intensive diffraction peak at 26.5° (2θ) corresponding to the interlayer spacing of about 0.34 nm. However, the peak completely disappeared upon oxidation of graphite to GO and a typical sharp peak at $2\theta = 10.0°$ with a corresponding interlayer spacing of 0.89 nm appeared at the XRD pattern of GO. Meanwhile, the relatively broad diffraction peak move to $2\theta = 24.0°$ with 0.37 nm d-spacing after reduction of GO to rGO. The variation of layer distance might be ascribed to the oxygen-containing functional group on the surface of GO introduced or removed, which suggested that the surface of GO may be grafted a lot of oxygen-containing groups.

Raman spectra is a powerful tool to investigate the structural change of carbon materials [38]. As shown in the Raman spectra (Fig. 3c), there were two prominent peaks corresponding to the D band and the G band. The D band corresponds to the stretching vibration of sp^3 carbon atoms inducing defects and disorders, while the G band is caused by the stretching vibration of sp^2 carbon atoms, which correspond to the first-order scattering of the E_{2g} mode. The I_D/I_G value of graphite was 0.35. After the graphite was oxidized to form GO, the value increased to 0.90. Additionally, the intensity of the D band of GO increased and exhibited a broader shape compared with that of graphite. It is suggested that the oxidation process changed the structure of graphite and the GO had a higher disorder degree than that of graphite, which meant that GO had more defects than graphite. Such a change of structure would offer more active sites for adsorption.

The element characterization and surface functional groups of GO was analyzed by XPS. According to the XPS spectrum of GO (Fig. 3d), deconvolution of the C 1s peak of GO resolved to a peak at 284.73 eV, which was attributed to the presence of C—C and C=C. The peaks at 286.82, 287.63, and 288.81 eV correlated to the carbon in C—O, the carbonyl carbon in C=O, and the carboxyl carbon in O—C=O, respectively. The XPS analysis indicated that the surface of GO not only existed sp^2 hybridized zone but also had a multitude of polar functional groups. These results implied that the material was quite hydrophilic.

3.2. E2 adsorption kinetics

Adsorption is a physicochemical process that involves mass transfer of a solute from liquid phase to the adsorbent surface [34]. In order to better understand the adsorption rate of adsorbent and the required time of the whole adsorption process, adsorption kinetics have been investigated. Fig. 4 presents the effect of contact time on the adsorption of E2 by graphene oxide nanosheets. It can be seen that the uptake of E2 rapidly increased in the first 1 h and then slowly increased until the adsorption equilibrium was reached within 12 h. According to the above study result, 8 h was chose for a sure contact time of the adsorption equilibrium in further adsorption studies.

To further investigate the adsorption mechanism, the results were analyzed by two conventional kinetic models, namely pseudo-first-order and pseudo-second-order model. The kinetic parameters and correlation coefficients (R^2) obtained from two models are listed in Table 1. The R^2 value of the pseudo-second-order model was much higher than that of the pseudo-first-order model. In addition, the little discrepancy between the experimental

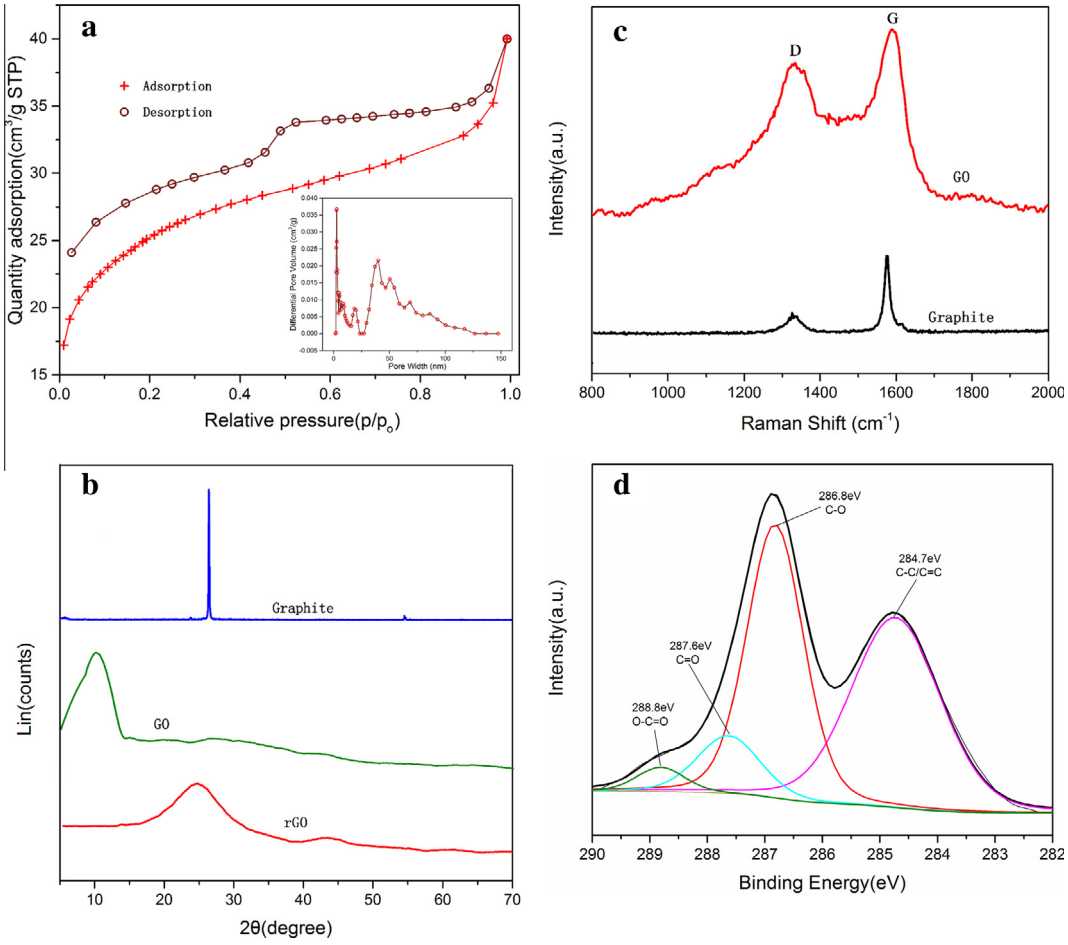

Fig. 3. (a) N2 adsorption–desorption isotherms of GO; (b) the XRD patterns of graphite, GO, and rGO; (c) Raman spectra of graphite and GO; (d) C1s XPS spectrum for the GO.

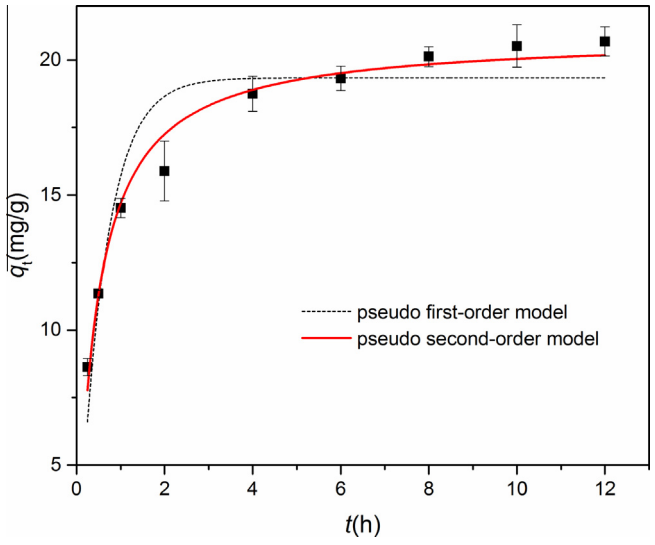

Fig. 4. Effect of contact time on the adsorption of E2 by GO: m/V = 0.1 mg/mL, C_{E2} = 2 mg/L, T = 298 K, pH = 7.0.

and the calculated adsorption capacity indicated that the pseudo-second-order kinetic model fitted E2 adsorption of GO better than the pseudo-first-order model. The adsorption process was better represented by the pseudo-second order model, which indicated that the chemisorption may be the rate-limiting mechanism of E2 adsorption. Thus, it was inferred that E2 was mainly adsorbed onto the surface of GO by chemical interaction, such as π–π interaction and hydrogen bonding.

Table 1
Kinetic parameters for adsorption of E2 on GO.

$q_{e,exp}$	Pseudo-first-order			Pseudo-second-order		
	$q_{e,1}$ (mg/g)	k_1 (1/h)	R^2	$q_{e,2}$ (mg/g)	k_2 (g/mg h)	R^2
20.69	19.34	1.67	0.869	20.89	0.11	0.976

3.3. E2 adsorption isotherm

The adsorption isotherm models are very useful to describe how the adsorbed molecules distribute on the adsorbents when the adsorption process reaches an equilibrium state [12]. Fig. 5 shows uptake of E2 by GO at three different temperatures. As can be seen, the adsorption capacity of GO increased sharply at the low initial concentration. This could be attributed to massive active sites which were readily accessible. However, the increasing trend became slow with further increase of initial concentration, which indicated that there are less available active sites at the end of the adsorptive process.

In order to study the mechanism of the adsorption equilibrium, Langmuir and Freundlich isotherm models were used to explore the adsorption process. Langmuir model can be used to describe homogeneous adsorption systems in which adsorption takes place on a homogeneous surface by a monolayer and equivalent sorption

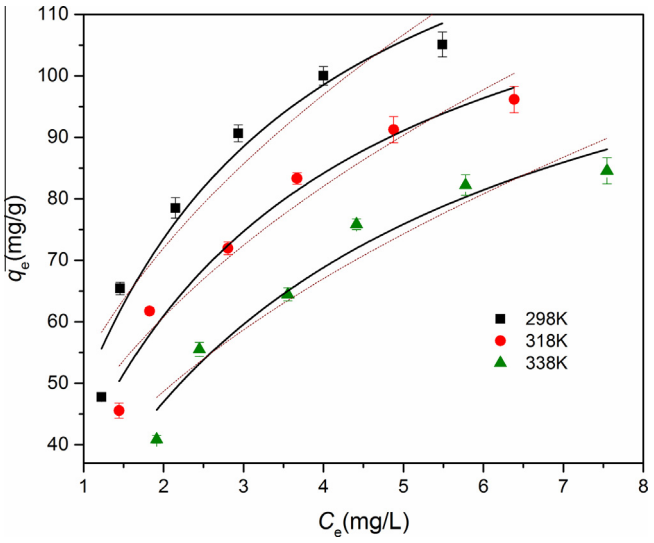

Fig. 5. Adsorption isotherms of E2 by GO at three different temperatures: m/V = 0.1 mg/mL, t = 8 h, pH = 7.0. The solid lines are the Langmuir model simulation; the dotted lines are the Freundlich model simulation.

energies [5]. While the Freundlich equation is put forward as an empirical equation which is used to describe heterogeneous systems and is not restricted to the formation of the monolayer [39]. The relative results simulated from the Langmuir and Freundlich models at three different temperatures are shown in Table 2. According to a comparison of the values of correlation coefficient (R^2), root mean square error (RMSE) and chi-square test (χ^2), the adsorption isotherm of E2 could be better described by Langmuir than Freundlich model. Thus, it was a monolayer adsorption that take place in the adsorption process. It also can be seen that the adsorption capacity (q_e) calculated from the Langmuir equation decreased with the increasing temperature from 298 K to 338 K.

In addition, there are several adsorbents that have been conducted to adsorption E2. Zaib et al. prepared single-walled carbon nanotubes and tested for E2 adsorption [11]. The adsorption capacities determined from the Langmuir isotherm were around 26 mg/g. Sun et al. investigated the adsorption of E2 on multiwalled carbon nanotubes (MWCNTs) and found that the maximum adsorption capacity close to 25 mg/g [12]. However, it can be seen from this study that GO exhibited a higher adsorption capacity (149.4 mg/g) than the adsorbents reported above [11,12]. Compared with carbon nanotubes, GO possesses an open-layered structure that has a completely accessible adsorption surface for organic molecules. Considering the oxygen content of GO (50.9%) [29], SWCNTs (0.9%) [40] and MWCNTs (about 23%) [41], GO remained more oxygen-containing functional groups on the surface which decrease the surface hydrophobicity. It may increase the dispersion of GO in water and also improve its adsorption capacity. Therefore, GO was an outstanding adsorbent in E2 pollution removal.

Table 2
Langmuir and Freundlich isotherm parameters for adsorption of E2 on GO.

T (K)		298	318	338
Langmuir	q_m (mg/g)	149.40	135.86	128.62
	K_L (L/mg)	0.484	0.407	0.287
	R^2	0.946	0.968	0.948
	RMSE	5.072	3.404	3.876
	χ^2	25.721	11.589	15.023
Freundlich	K_f (L/mg)	53.42	45.03	35.35
	N	0.43	0.43	0.46
	R^2	0.888	0.927	0.895
	RMSE	7.321	5.163	5.486
	χ^2	53.604	26.657	30.09

3.4. E2 adsorption thermodynamic

The thermodynamic parameters were calculated from the data in Fig. 4 by Eqs. (6) and (7) and the results are shown in Table 3. The values of ΔG° were found to be negative at all temperatures and became more negative with decreasing temperature, which indicated that the adsorption was a spontaneous process and the lower temperature was beneficial to the adsorption of E2 onto GO. The negative ΔH° value implied that the adsorption reaction was exothermic, and it is the reason why the adsorption capacity of E2 decrease with increasing in temperature. The negative ΔS° value revealed the decreased randomness at adsorbate–adsorbent interface during the adsorption progress.

3.5. Effect of solution pH

The solution pH value is one of the most important parameter in determining the adsorption characteristics of adsorbents, since it can change the surface charge of the adsorbent and the speciation distribution of adsorbate in solution. Fig. 6 shows the effect of initial pH on E2 adsorption by GO with pH ranging 3.0–12.0. It was found that the uptake of E2 by GO decreased slowly as pH value increased from 3.0 to 7.0. Above pH 7.0, there was a different trend that the capacity of adsorption decreased rapidly and even decreased to approximately 17 mg/g at pH 12.0. These phenomena may be resultant from the change of the surface charge of graphene oxide and the speciation of E2 at different pH values. As can also be seen from the Fig. 6, the zeta potentials of GO kept negative and decreased all along at the whole pH range. It illustrated that the charge of GO was negative and the negative charge would be enhanced with increasing pH. As reported, the pK_a of E2 is 10.4 [42]. Therefore, E2 would start deprotonating around pH 10.0. Sun et al. reported that E2 was is prone to dissociation in weakly alkaline solutions [12]. After deprotonation, E2 molecules also became negative. Thus, the repulsive electrostatic interaction established between the negative surface charge of GO and the E2 anion might lead to the low adsorptive capacity of GO in the range of alkaline.

3.6. Effect of ionic strength

It is well known that industrial sewage contains not only organic-pollutants but also some of salts, which may affect the removal of pollutants [32]. Thus, the effect of solution ionic strength on the sorption of E2 by GO was investigated by a series of experimental studies constructed by varying concentrations of NaCl solutions from 0 to 0.1 M. As depicted in Fig. 7, it can be found that the uptake of E2 by GO was improved in the presence of NaCl. Two potential impacts might exist in this process: (1) increasing ionic strength enhanced the activity coefficient of hydrophobic organic compounds and result in decreasing in their solubility (i.e. salting out effect), which is favorable for E2 adsorption [43]; and (2) the ions may infiltrate into the diffuse double layer over GO surfaces and eliminate the repelling interaction between the

Table 3
Thermodynamic parameters of E2 adsorption on GO.

T (K)	$\ln K^0$	ΔG^0 (kJ/mol)	ΔS^0 (J/K mol)	ΔH^0 (kJ/mol)
298	1.39	−3.43	−0.72	−3.65
318	1.29	−3.42		
338	1.21	−3.40		

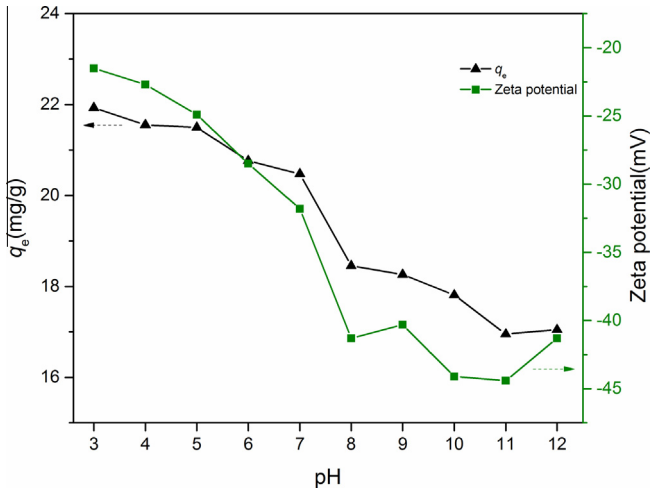

Fig. 6. Effect of the solution pH: m/V = 0.1 mg/mL, C_{E2} = 3 mg/L, T = 298 K, t = 8 h.

adsorbents, resulting in promoting the formation of a more compact aggregation structure (i.e. squeezing-out), which is unfavorable for E2 sorption [44]. When the adsorption capacity increased rapidly at the NaCl concentration below 0.001 M, it is suggested that the salting-out effect was consistently greater than the squeezing-out effect. However, when the NaCl concentration was >0.001 M, the adsorption capacity decreased slightly, which indicated that the salting-out effect was decreasing continuously.

3.7. Effect of background electrolyte

The effect of background electrolyte cations such as NaCl, KCl, $MgCl_2$ and $CaCl_2$ on the E2 adsorption by GO were examined, and the results are shown in Fig. 8(a). It can be found that the adsorption capacity of E2 adsorbed to GO in the presence of divalent cations (Mg^{2+} and Ca^{2+}) lower than monovalent cations (Na^+ and K^+). This phenomenon can be explained by the above squeezing-out effect which is more when divalent cations are present due to their high polarizing power. Fig. 8(b) showed the effect of background electrolyte anions on the E2 adsorption onto GO in NaCl, $NaNO_3$, Na_2SO_4 and Na_3PO_4 solutions, respectively. It was observed

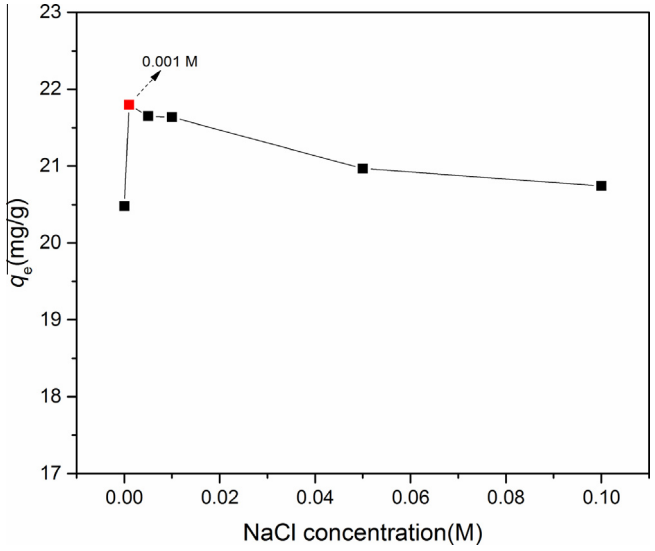

Fig. 7. Effect of the ionic strength: m/V = 0.1 mg/mL, C_{E2} = 3 mg/L, T = 298 K, t = 8 h, pH = 7.0.

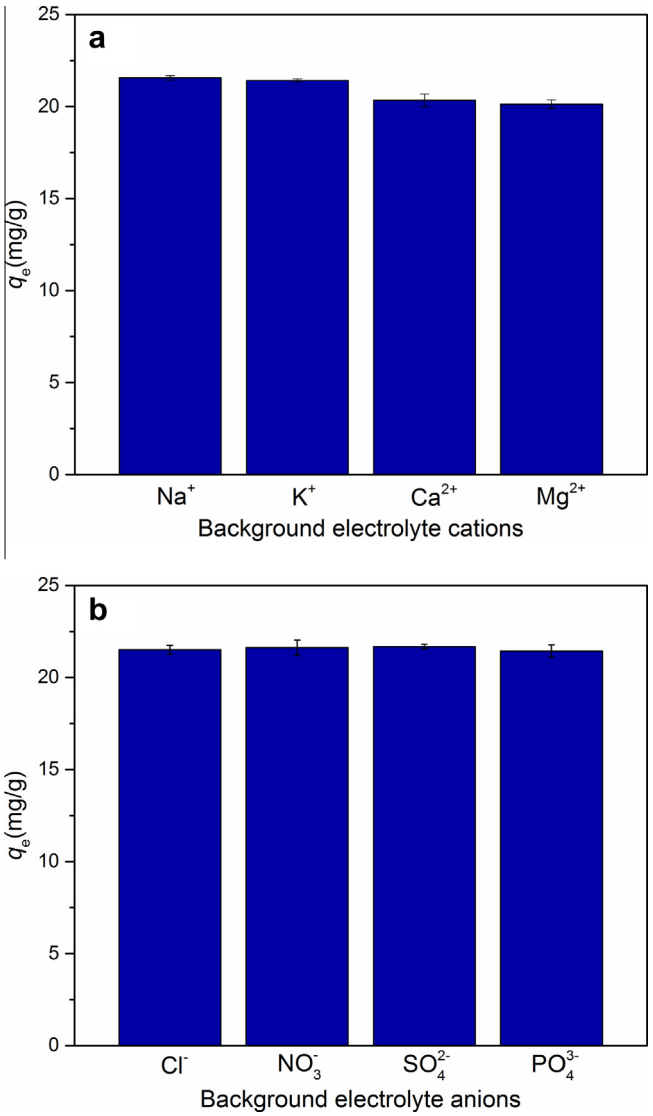

Fig. 8. (a) Effect of background electrolyte cations; (b) Effect of background electrolyte anions: m/V = 0.1 mg/mL, C_{E2} = 3 mg/L, T = 298 K, t = 8 h, pH = 7.0.

that the adsorption capacity of E2 adsorbed to GO in presence of these investigated anions were not significantly different ($P > 0.05$), as compared to chloride ions. These phenomena may be mainly attributed to the electrostatic repulsion between the negatively charged GO surface and the anions, which result in minimal adsorption of anions to GO surfaces.

3.8. Effect of humic acid

Humic substances such as humic and fulvic acids are widespread in soil and water and they are derived from the decomposition of natural organic compounds [45]. The change of q_e in the presence of humic acid (HA) was showed in Fig. 9. The adsorption capacity decreased with the increase in humic acid concentration. It is known that humic acid tend to contain a lot of functional groups including phenolic hydroxyls and carboxylates [46]. The dissociation of these groups in aqueous solution leads to the formation of negative charges bound which can interact with various organic pollutants. Thus, the decrease of E2 adsorption might be explained by the formation of soluble E2-HA complexes in aqueous media [30]. In addition, the strong interaction of HA with GO

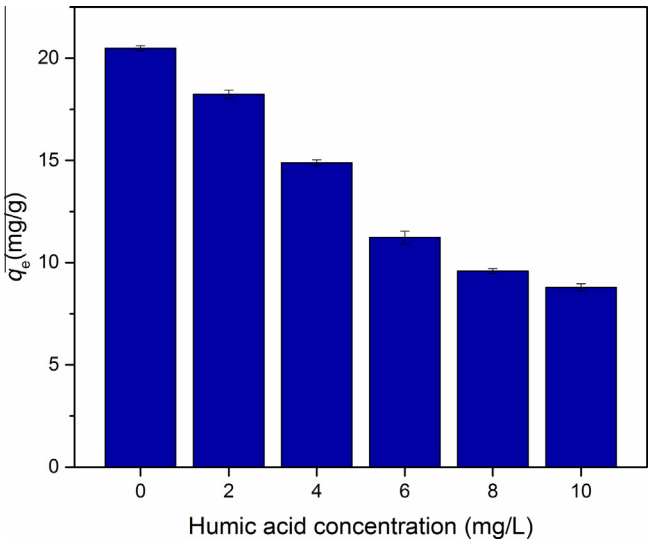

Fig. 9. Effect of the humic acid: m/V = 0.1 mg/mL, C_{E2} = 3 mg/L, T = 298 K, t = 8 h, pH = 7.0.

through π–π interactions can occupy parts of surface sorption sites of GO and thereby results in the decrease of E2 adsorption capacity of graphene oxide nanosheets [30].

3.9. Desorption and regeneration analysis

To assess the reusability and cost effectiveness of any adsorbent, it is rather important to examine its performance through simulated desorption/regeneration cycles [47]. From Fig. 10, it was observed that in the first cycle the adsorption ability of E2 onto the as prepared GO was 20.12 mg/g at 298 K and pH 7.0. After five adsorption/desorption cycles, however, the adsorption ability of E2 onto the recycled GO still remains at 19.27 mg/g, which just reduced by 5.86% compared with that of the first cycle. This shows that GO could be an economical, efficient and potential adsorbent for E2 removal due to the excellent regeneration performance of numerous cycles. However, the reduction adsorbed amount of E2 by GO may be attributed to loss of surface functional groups which could in turn be used to treatment with strong alkali acting as desorption medium [23].

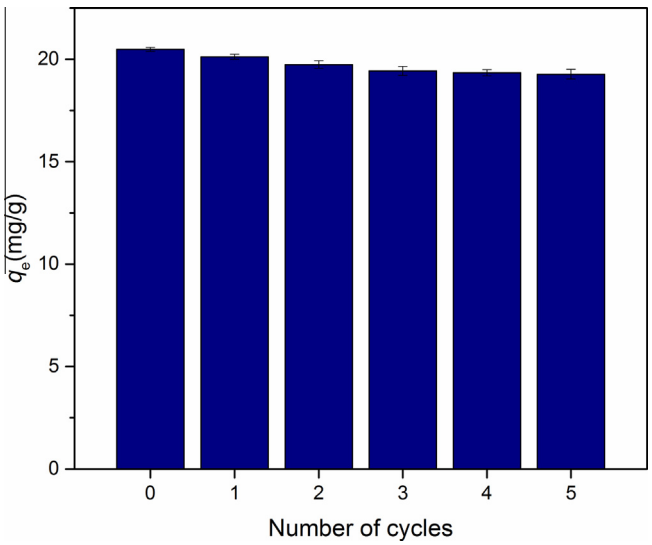

Fig. 10. Fifth consecutive desorption/adsorption cycles of GO for removal: m/V = 0.1 mg/mL, C_{E2} = 3 mg/L, T = 298 K, t = 8 h, pH = 7.0.

3.10. Adsorption mechanism

Surfaces of GO shows the π-electron acceptor or donor properties due to containing both the π-electron-depleted regions (i.e. the presence of defects or functional groups) and π-electron-rich regions (i.e. the delocalization of π electrons) [29]. E2, with the several fused aromatic rings, is π electron-rich. The substitution with a strong electron-donating —OH group further enhances the π electron density of the aromatic rings [48]. Thus, These π electrons can easily interact with the π electrons of benzene rings on GO due to the larger and smoother surface and π–π interaction is likely in effect for the adsorption of E2 onto GO. Besides, there were abundant surface oxygen-containing groups in GO such as hydroxyl groups which can undergo hydrogen bonds with hydroxyl groups of E2.

To probe the molecular interaction of E2 with GO, the FTIR spectra of GO after E2 adsorption is shown in Fig. 11. As can be seen from the FTIR spectra, the intense peak at 3407 cm^{-1} was associated with the skeletal vibration of O—H groups. The peak at 1726 cm^{-1} corresponded to C═O bonds in carboxylic acid and carbonyl moieties. The peak at 1624 cm^{-1} can be attributed to the stretching vibration of aromatic C═C bonds. The peak at around 1402 cm^{-1} was assigned to the appearance of carboxyl (O═C—O) bonds. The peak at 1225 cm^{-1} belonged to epoxy (C—O—C) bonds. The peak at around 1051 cm^{-1} referred to alkoxy (C—O) bonds. Compared to GO, it can be found that quite a few new peaks were introduced into the FTIR spectrum of GO after E2 adsorption. These intensely peaks at 500–1200 cm^{-1} were in accordance with the peaks from the FTIR spectrum of E2, which indicated that a multitude of E2 molecules had been adsorbed on the surface of GO. In addition, the peaks corresponding to the skeletal vibration of C═C bonds also shifted from 1624 to 1635 cm^{-1} after adsorption of E2. So it is confirmed that there was π–π interaction between E2 and GO [29]. Moreover, the peaks of the alkoxy C—O bending vibration shifted from 1051 to 1042 cm^{-1}, and the peaks of the carboxyl O—H bending vibration of GO shifted from 3407 to 1378 cm^{-1} and formed strong and wide associating O—H after adsorption with E2. The clear changes reflected by FTIR suggested that interactions between the E2 molecules and oxygen-containing functional groups of GO occurred and there was hydrogen bonds

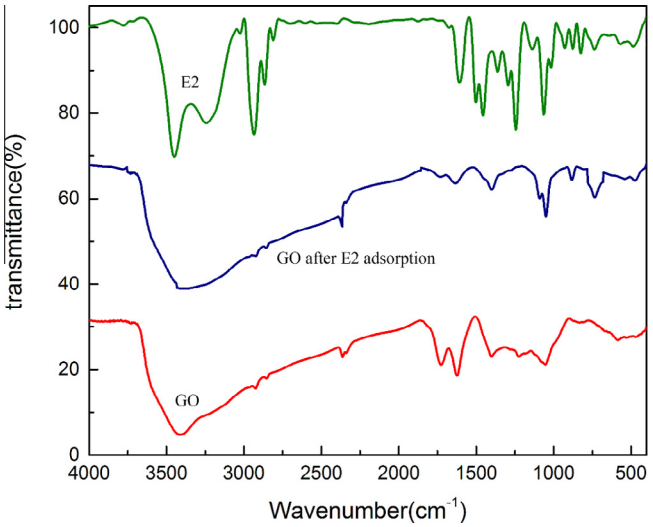

Fig. 11. FTIR spectra of GO, E2, and GO after E2 adsorption.

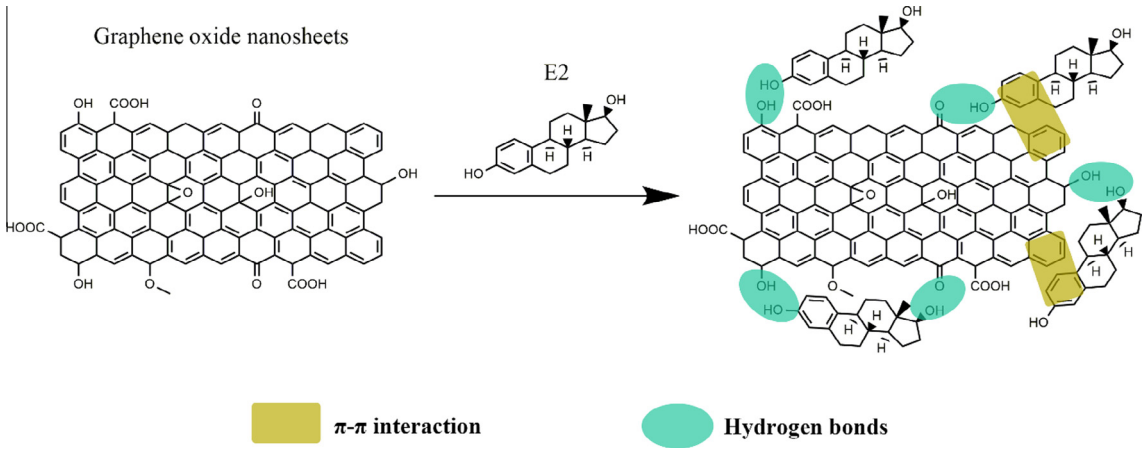

Fig. 12. Schematic illustration of adsorption mechanisms by GO.

between the E2 and GO. Therefore, it is demonstrated the presence of the π–π interaction and hydrogen bonds between E2 and GO, and the adsorption mechanism could be illustrated by Fig. 12.

4. Conclusions

Graphene oxide nanosheets showed excellent adsorption capacity for E2. The maximum adsorption capacity (q_m) of GO for E2 calculated from the Langmuir isotherm was 149.4 mg/g at 298 K, which was the highest values of E2 adsorption compared to that of other adsorbents reported before. The kinetics and isotherm parameters can be well described by the pseudo-second-order kinetic model and the Langmuir isotherm, respectively. The adsorption process was exothermic and spontaneous. The large adsorption affinity of GO for E2 might be mainly due to π–π interactions and hydrogen bonds. The adsorption capacity was slight affected by the solution pH. The presence of NaCl in the solution was favorable for the E2 adsorption and the optimum results were observed in the 0.001 M concentration of NaCl. Besides, the adsorption capacity in the presence of background electrolyte divalent cations (Mg^{2+} and Ca^{2+}) lower than monovalent cations (Na^+ and K^+). As compared to chloride ions, however, the adsorption capacity in presence of other background electrolyte anions (NO_3^-, SO_4^{2-}, and PO_4^{3-}) were not significantly different. The adsorption capacity slight decreased with the increase in humic acid concentration. In addition, the adsorbent could be regenerated and reused by sodium hydroxide and acetone. Thus, GO could be a cost-effective, efficient and potential adsorbent for E2 removal.

Acknowledgements

This project was supported by the National Natural Science Foundation of China (Grant Nos. 41271332 and 51478470).

References

[1] A.C. Johnson, E. Dumont, R.J. Williams, R. Oldenkamp, I. Cisowska, J.P. Sumpter, Do concentrations of ethinylestradiol, estradiol, and diclofenac in European rivers exceed proposed EU environmental quality standards, Environ. Sci. Technol. 47 (2013) 12297–12304.
[2] Z. Fan, J. Hu, W. An, M. Yang, Detection and occurrence of chlorinated byproducts of bisphenol A, nonylphenol, and estrogens in drinking water of china: comparison to the parent compounds, Environ. Sci. Technol. 47 (2013) 10841–10850.
[3] C. Qin, D. Troya, C. Shang, S. Hildreth, R. Helm, K. Xia, Surface catalyzed oxidative oligomerization of 17β-estradiol by Fe^{3+}-saturated montmorillonite, Environ. Sci. Technol. 49 (2014) 956–964.
[4] K.L. Thorpe, G. Maack, R. Benstead, C.R. Tyler, Estrogenic wastewater treatment works effluents reduce egg production in fish, Environ. Sci. Technol. 43 (2009) 2976–2982.
[5] F. Wang, W. Sun, W. Pan, N. Xu, Adsorption of sulfamethoxazole and 17β-estradiol by carbon nanotubes/$CoFe_2O_4$ composites, Chem. Eng. J. 274 (2015) 17–29.
[6] W. Zhang, Y. Li, Q. Wang, C. Wang, P. Wang, K. Mao, Performance evaluation and application of surface-molecular-imprinted polymer-modified TiO_2 nanotubes for the removal of estrogenic chemicals from secondary effluents, Environ. Sci. Pollut. Res. 20 (2013) 1431–1440.
[7] P.M. Bradley, Effect of light on biodegradation of estrone, 17β-estradiol, and 17α-ethinylestradiol in stream sediment, J. Am. Water Resour. Assoc. 50 (2014) 334–342.
[8] C.L. Hu, W.F. Wang, Y.H. Hsieh, Study on 17β-Estradiol (E2) removal in wastewater by continuous-flow advanced treatment and economic benefit evaluation, J. Chem. Eng. Jpn. 48 (2015) 458–462.
[9] Y. Zhang, J.L. Zhou, Removal of estrone and 17β-estradiol from water by adsorption, Water Res. 39 (2005) 3991–4003.
[10] Y. Yoon, P. Westerhoff, S.A. Snyder, M. Esparza, HPLC-fluorescence detection and adsorption of bisphenol A, 17β-estradiol, and 17α-ethynyl estradiol on powdered activated carbon, Water Res. 37 (2003) 3530–3537.
[11] Q. Zaib, I.A. Khan, N.B. Saleh, J.R.V. Flora, Y.G. Park, Y. Yoon, Removal of bisphenol A and 17β-estradiol by single-walled carbon nanotubes in aqueous solution: adsorption and molecular modeling, Water Air Soil Poll. 223 (2012) 3281–3293.
[12] W. Sun, K. Zhou, Adsorption of 17β-estradiol by multi-walled carbon nanotubes in natural waters with or without aquatic colloids, Chem. Eng. J. 258 (2014) 185–193.
[13] E.A. McCallum, H. Hyung, T.A. Do, C.H. Huang, J.H. Kim, Adsorption, desorption, and steady-state removal of 17β-estradiol by nanofiltration membranes, J. Membr. Sci. 319 (2008) 38–43.
[14] M. Le Noir, A.S. Lepeuple, B. Guieysse, B. Mattiasson, Selective removal of 17β-estradiol at trace concentration using a molecularly imprinted polymer, Water Res. 41 (2007) 2825–2831.
[15] S. Latil, L. Henrard, Charge carriers in few-layer graphene films, Phys. Rev. Lett. 97 (2006) 036803.
[16] C. Lee, X. Wei, J.W. Kysar, J. Hone, Measurement of the elastic properties and intrinsic strength of monolayer graphene, Science 321 (2008) 385–389.
[17] J.C. Meyer, A.K. Geim, M.I. Katsnelson, K.S. Novoselov, T.J. Booth, S. Roth, The structure of suspended graphene sheets, Nature 446 (2007) 60–63.
[18] A.S.K. Kumar, S.J. Jiang, Preparation and characterization of exfoliated graphene oxide-L-cystine as an effective adsorbent of Hg (II) adsorption, RSC Adv. 5 (2015) 6294–6304.
[19] H.K. Seo, M. Song, S. Ameen, M.S. Akhtar, H.S. Shin, New counter electrode of hot filament chemical vapor deposited graphene thin film for dye sensitized solar cell, Chem. Eng. J. 222 (2013) 464–471.
[20] M. Mirnezhad, R. Ansari, H. Rouhi, M. Faghihnasiri, Graphene-based sensors for monitoring strain: a first-principles density functional theory analysis, Int. J. Chemoinform. Chem. Eng. 3 (2013) 74–83.
[21] S. Park, R.S. Ruoff, Chemical methods for the production of graphenes, Nat. Nanotechnol. 4 (2009) 217–224.
[22] R. Sitko, E. Turek, B. Zawisza, E. Malicka, E. Talik, J. Heimann, et al., Adsorption of divalent metal ions from aqueous solutions using graphene oxide, Dalton Trans. 42 (2013) 5682–5689.
[23] S. Pavagadhi, A.L.L. Tang, M. Sathishkumar, K.P. Loh, R. Balasubramanian, Removal of microcystin-LR and microcystin-RR by graphene oxide: adsorption and kinetic experiments, Water Res. 47 (2013) 4621–4629.
[24] H. Yan, H. Wu, K. Li, Y. Wang, X. Tao, H. Yang, et al., Influence of the surface structure of graphene oxide on the adsorption of aromatic organic compounds from water, ACS Appl. Mater. Interfaces 7 (2015) 6690–6697.

[25] H. Yan, X. Tao, Z. Yang, K. Li, H. Yang, A. Li, et al., Effects of the oxidation degree of graphene oxide on the adsorption of methylene blue, J. Hazard. Mater. 268 (2014) 191–198.
[26] O. Moradi, V.K. Gupta, S. Agarwal, I. Tyagi, M. Asif, A.S.H. Makhlouf, et al., Characteristics and electrical conductivity of graphene and graphene oxide for adsorption of cationic dyes from liquids: kinetic and thermodynamic study, J. Ind. Eng. Chem. 28 (2015) 294–301.
[27] G.P. Kingori, J.Z. Sun, Z.H. Liao, R.W. Si, Adsorption and removal of triphenylmethane dyes from water by magnetic reduced graphene oxide, Water Sci. Technol. 70 (2014) 1663–1669.
[28] H. Wang, Y. Liu, G. Zeng, X. Hu, X. Hu, T. Li, et al., Grafting of β-cyclodextrin to magnetic graphene oxide via ethylenediamine and application for Cr(VI) removal, Carbohydr. Polym. 113 (2014) 166–173.
[29] J. Wang, Z. Chen, B. Chen, Adsorption of polycyclic aromatic hydrocarbons by graphene and graphene oxide nanosheets, Environ. Sci. Technol. 48 (2014) 4817–4825.
[30] G. Zhao, J. Li, X. Ren, C. Chen, X. Wang, Few-layered graphene oxide nanosheets as superior sorbents for heavy metal ion pollution management, Environ. Sci. Technol. 45 (2011) 10454–10462.
[31] Z. Wu, H. Zhong, X. Yuan, H. Wang, L. Wang, X. Chen, et al., Adsorptive removal of methylene blue by rhamnolipid-functionalized graphene oxide from wastewater, Water Res. 67 (2014) 330–344.
[32] J. Xu, L. Wang, Y. Zhu, Decontamination of bisphenol A from aqueous solution by graphene adsorption, Langmuir 28 (2012) 8418–8425.
[33] J. Han, W. Qiu, J. Hu, W. Gao, Chemisorption of estrone in nylon microfiltration membranes: adsorption mechanism and potential use for estrone removal from water, Water Res. 46 (2012) 873–881.
[34] X. Hu, J. Wang, Y. Liu, X. Li, G. Zeng, Z. Bao, et al., Adsorption of chromium (VI) by ethylenediamine-modified cross-linked magnetic chitosan resin: isotherms, kinetics and thermodynamics, J. Hazard. Mater. 185 (2011) 306–314.
[35] L. Zhang, X. Li, Y. Huang, Y. Ma, X. Wan, Y. Chen, Controlled synthesis of few-layered graphene sheets on a large scale using chemical exfoliation, Carbon 48 (2010) 2367–2371.
[36] L. Zhang, J. Liang, Y. Huang, Y. Ma, Y. Wang, Y. Chen, Size-controlled synthesis of graphene oxide sheets on a large scale using chemical exfoliation, Carbon 47 (2009) 3365–3368.
[37] J.J. Pignatello, Characterization of aromatic compound sorptive interactions with black carbon (charcoal) assisted by graphite as a model, Environ. Sci. Technol. 39 (2005) 2033–2041.
[38] C. Zhang, L. Wu, D. Cai, C. Zhang, N. Wang, J. Zhang, et al., Adsorption of polycyclic aromatic hydrocarbons (fluoranthene and anthracenemethanol) by functional graphene oxide and removal by pH and temperature-sensitive coagulation, ACS Appl. Mater. Interfaces 5 (2013) 4783–4790.
[39] S. Sheshmani, A. Ashori, S. Hasanzadeh, Removal of acid orange 7 from aqueous solution using magnetic graphene/chitosan: a promising nano-adsorbent, Int. J. Biol. Macromol. 68 (2014) 218–224.
[40] Y. Zhou, O.G. Apul, T. Karanfil, Adsorption of halogenated aliphatic contaminants by graphene nanomaterials, Water Res. 79 (2015) 57–67.
[41] V. Datsyuk, M. Kalyva, K. Papagelis, J. Parthenios, D. Tasis, A. Siokou, et al., Chemical oxidation of multiwalled carbon nanotubes, Carbon 46 (2008) 833–840.
[42] Y. Lee, J. Yoon, U. Von Gunten, Kinetics of the oxidation of phenols and phenolic endocrine disruptors during water treatment with ferrate (Fe (VI)), Environ. Sci. Technol. 39 (2005) 8978–8984.
[43] S. Zhang, T. Shao, S.S.K. Bekaroglu, T. Karanfil, Adsorption of synthetic organic chemicals by carbon nanotubes: effects of background solution chemistry, Water Res. 44 (2010) 2067–2074.
[44] Y. Zhang, S.F. Ali, E. Dervishi, Y. Xu, Z. Li, D. Casciano, et al., Cytotoxicity effects of graphene and single-wall carbon nanotubes in neural phaeochromocytoma-derived PC12 cells, ACS Nano 4 (2010) 3181–3186.
[45] J.J. Pignatello, S. Kwon, Y. Lu, Effect of natural organic substances on the surface and adsorptive properties of environmental black carbon (char): attenuation of surface activity by humic and fulvic acids, Environ. Sci. Technol. 40 (2006) 7757–7763.
[46] J. Peuravuori, K. Pihlaja, Molecular size distribution and spectroscopic properties of aquatic humic substances, Anal. Chim. Acta 337 (1997) 133–149.
[47] A.R. Binupriya, M. Sathishkumar, D. Kavitha, K. Swaminathan, S.E. Yun, Aerated and rotated mode decolorization of a textile dye solution by native and modified mycelial biomass of Trametes versicolor, J. Chem. Technol. Biotechnol. 82 (2007) 350–359.
[48] L. Ji, W. Chen, Z. Xu, S. Zheng, D. Zhu, Graphene nanosheets and graphite oxide as promising adsorbents for removal of organic contaminants from aqueous solution, J. Environ. Qual. 42 (2013) 191–198.